Table 6.2.1 presents the fitted values for the curvature of the wavefront, the angular misalignment, the quality of the fit (through the correlation coefficient r^2), and the radius of curvature calculated from the curvature in this case. The quality of the linear regression fits shows that our previous assumption of the measured wavefront being spherical was close to reality. This same conclusion may be drawn from the linear shapes of Figures 6.2.8c to 6.2.8e.

Table 6.2.1: Linear regression results for the X and Y directions of the non-microstepped and microstepped experiments, assuming a curve $y=C\xi+K$, where ξ may be either x_R or y_R, and y either u or v. C is the curvature, K the angular misalignment (see text), r^2 the correlation coefficient and R the measured radius of curvature of the wavefront at the Ronchi ruling.

Sample P175 A	**C(mm^{-1})**	**K(rad)**	**r^2**	**R(mm)**
u(x_R); non-µstepped	$-2.4690\ 10^{-2}$	$2.8792\ 10^{-2}$	0.999935	40.50
v(y_R) ;non-µstepped	$-2.4819\ 10^{-2}$	$1.3770\ 10^{-3}$	0.999963	40.29
u(x_R); µstepped	$-2.4654\ 10^{-2}$	$2.8750\ 10^{-2}$	0.999905	40.56
v(y_R); µstepped	$-2.4807\ 10^{-2}$	$1.3486\ 10^{-3}$	0.999964	40.31

Small differences (around 5%) may be appreciated in the values of curvature measured along the X and Y directions. These differences are a consequence of the different pixel angular size along both directions, as was described in Section 4.3.1. Any errors in the measurement of this parameter (which also includes the effects of the objective lens and the frame-grabber) have been shown to be quite influent in the measured value in the error analysis of the slope measurements (See Table 4.3.1).

The misalignment term of the linear regression proves to be greater along the X axis than along the Y axis, confirming what can be seen in Fig. 6.2.8a and 6.2.8b. This error, associated with the misalignment or tilt of the sampled surface relative to the incident wavefront, may be seen to be quite large along the X axis in this sample. The quality of all linear regressions is depicted by its correlation coefficient, showing how experimental results very closely follow a line both in microstepped and non-microstepped results.

At this stage it may already be seen how the difference between microstepped and non-microstepped measurements of curvature is very small. Microstepping was proposed in order to improve the sampling in the topographic reconstructions of the

surface, but the fitted curvature and origin values should only be slightly altered by the presence of a greater number of data points if the correlation coefficients are good.

These measured position and slope values of the wavefront at the Ronchi ruling plane are then ray-traced to the plane tangent to the surface at its vertex, yielding a set of (x_S,y_S,u,v) values, where (u,v) are still the measured slopes of the ray impinging on the Ronchi ruling, and (x_S,y_S) the position where that ray incides on the plane tangent to the surface. Table 6.2.2 gives the results of curvature and angular misalignment around each axis obtained when curve-fitting the corresponding slope and position values at the tangent plane to the sample surface. These measurements correspond to curvature and angular misalignment of the wavefront reflected at the sample surface, once again assuming the wavefront has a spherical shape, and linear shapes of the u(x_S) and v(y_S) curves may therefore be expected. The $y_S(x_S)$, u(x_S) and v(y_S) curves are presented in Fig. 6.2.9.

Table 6.2.2: Linear regression results for the X and Y directions of the non-microstepped and microstepped experiments at the tangent plane to the sample surface, assuming a $y=C\xi+k$ curve, where ξ may be either x_S or y_S, and y either u or v. C stands for curvature, K for angular misalignment, r^2 for the correlation coefficient and R for the radius of curvature of the reflected wavefront.

Sample P175 A	C(mm^{-1})	K(rad)	r^2	R(mm)
u(x_S) ; non-μstepped	$6.6750\ 10^{-3}$	$-4.4088\ 10^{-3}$	0.999998	149.81
v(y_S) ;non-μstepped	$6.6679\ 10^{-3}$	$-2.2104\ 10^{-4}$	0.999999	149.97
u(x_S); μstepped	$6.6759\ 10^{-3}$	$-4.4105\ 10^{-3}$	0.999997	149.79
v(y_S); μstepped	$6.6684\ 10^{-3}$	$-2.0511\ 10^{-4}$	0.999999	149.96

One of the most visible features when comparing Fig. 6.2.8 and Fig. 6.2.9 is the inversion of the slope of the respective slope against position curves. This inversion is a consequence of our experimental conditions, which work out of focus, that is, with a theoretical focusing point prior to the incidence of the light rays onto the Ronchi ruling. Another important difference between the two figures is the great increase in the sampled area as a consequence of the divergence of the light beam. The value obtained at this point is the final sampled area of the surface, which amounts to 204mm^2, while the area covered on the Ronchi ruling was just of 19.4mm^2.

Fig. 6.2.9: Measured data of the reflected wavefront at the plane tangent to the sampled surface; (a) $y_S(x_S)$ without microstepping; (b) $y_S(x_S)$ with microstepping; (c) $u(x_S)$ without microstepping; (d) $u(x_S)$ with microstepping; (e) $v(y_S)$ without microstepping; (f) $v(y_S)$ with microstepping.

Table 6.2.2 shows how the value of the angular misalignment term of the reflected wavefront is one order of magnitude smaller at the plane tangent to the surface, together with an improvement of the quality of the fits, which are even closer to perfect lines than the ones obtained on the Ronchi ruling plane. The most remarkable feature to point out in Table 6.2.2, however, is the measured curvature of the reflected wavefront at the surface. This value can still not properly be called the surface curvature, as this must be obtained from fitting the local normals to the surface to the corresponding position of the surface values, but this curvature of the reflected wavefront will be shown to be very close to the actual curvature of the surface.

Following Eq.4.2.4, the local normals to the surface can be obtained from the measured data on the tangent plane to the surface and from a set of known parameters of the experimental setup. Table 6.2.3 presents the final results obtained from the two-dimensional fitting of the $N_X(x_S)$ and $N_Y(y_S)$ curves, which are shown in Fig.6.2.10. The $y_S(x_S)$ graphs for the microstepped and non-microstepped experiment are not presented as they have already been plotted in Fig.6.2.9a and Fig.6.2.9b.

Table 6.2.3: Linear regression results for the X and Y directions of the non-microstepped and microstepped experiments, assuming a curve $y=C\xi+k$, where ξ may be either x_S or y_S, and y either N_X or N_Y. C is the curvature, K the angular misalignment, r^2 the correlation coefficient and R the measured surface's radius of curvature.

Sample P175 A	C(mm^{-1})	K(rad)	r^2	R(mm)
$N_X(x_S)$; non-μstepped	$6.6750\ 10^{-3}$	$-4.4088\ 10^{-3}$	0.999998	149.81
$N_Y(y_S)$;non-μstepped	$6.6678\ 10^{-3}$	$-2.2104\ 10^{-4}$	0.999999	149.97
$N_X(x_S)$; μstepped	$6.6759\ 10^{-3}$	$-4.4105\ 10^{-3}$	0.999997	149.79
$N_Y(y_S)$; μstepped	$6.6684\ 10^{-3}$	$-2.0516\ 10^{-4}$	0.999999	149.96

It may be seen that the $N_X(x_S)$ and $N_Y(y_S)$ (Fig. 6.2.10c and Fig. 6.2.10d) curves, and the $u(x_S)$ and $v(y_S)$ curves (Fig. 6.2.9c and Fig. 6.2.9d) are very similar. In fact, very slight differences may only be seen in their fitted curvature and angular misalignment values; these differences are listed as absolute values in Table 6.2.4. The maximum differences in the curvature values fitted between the two pairs of data are as small as $10^{-7}mm^{-1}$, yielding minimum modifications in the measured radius of curvature values which stay beyond the experimental uncertainties of our setup. The differences obtained using the local normals to the surface instead of the slopes of the reflected wavefront

are very small, but were taken into account in the data processing on behalf of the physical suitability of a surface reconstruction from its measured local normals. The coincidence of the two graphs is, of course, a consequence of the closeness of the light source to the center of curvature of the spherical surface, which yields very small angular differences between incident rays, local normals and reflected rays.

Fig. 6.2.10: Measured data of the sampled surface: (a) $N_X(x_S)$ without microstepping; (b) $N_X(x_S)$ with microstepping; (c) $N_Y(y_S)$ without microstepping; (d) $N_Y(y_S)$ with microstepping.

Table 6.2.4: Differences in the fitted values of the $u(x_S)$ and the $N_X(x_S)$ curves, and of the $v(y_S)$ and the $N_Y(y_S)$ curves, negligible under our experimental accuracy. Differences are shown without their sign.

Sample P175 A	**DC(mm^{-1})**	**DK(rad)**	**DR(mm)**
$u(x_S)$-$N_X(x_S)$ non-μstep.	$4\ 10^{-9}$	$1\ 10^{-8}$	$9\ 10^{-5}$
$v(y_S)$-$N_Y(y_S)$ non-μstep.	$1\ 10^{-9}$	$2\ 10^{-9}$	$2\ 10^{-5}$
$u(x_S)$-$N_X(x_S)$ μstepped	$9\ 10^{-9}$	$1\ 10^{-7}$	$2\ 10^{-4}$
$v(y_S)$-$N_Y(y_S)$ μstepped	$5\ 10^{-9}$	$5\ 10^{-8}$	$1\ 10^{-4}$

No noticeable variations of the measured radius of curvature are thus observed with the accuracy involved in our setup, when comparing the fitted values obtained using the components of the local normal to the surface and the ones obtained using the slopes along both axes of the reflected wavefront.

However, the angular error introduced when confusing the local normal and the slope of the wavefront should be greater under our experimental conditions with the light source close to the surface's center of curvature than the error introduced when confusing the tangent plane to the surface at its vertex with the surface itself, as may be seen in Fig. 6.2.11. This tangent plane assumption was used in the ray-tracing step previously performed in order to simplify calculations by making plane to plane ray propagation. As the angular error of this approximation is less significant, the error in the measured curvature involved should also be expected to be smaller.

In order to confirm this question, tests were made of iterative algorithms which, after the first topographic reconstruction, ray-traced again from the initial measured position and slope values on the Ronchi ruling plane to the best fit of the first reconstructed surface, yielding a second topographic reconstruction. However, the variation in the local normals and slopes obtained in both surface reconstruction procedures was so small that it did not affect the final measured curvature at all. These iterative algorithms were abandoned as they needed to assume the kind of surface being tested, involved a very large increase in computation time and did not improve the quality of the measurement in any way.

Fig. 6.2.11: The angular error introduced when confusing the normal to the surface with the direction of the reflected wavefront is much greater than the error introduced in the normal when propagating to the tangent plane instead of to the real surface

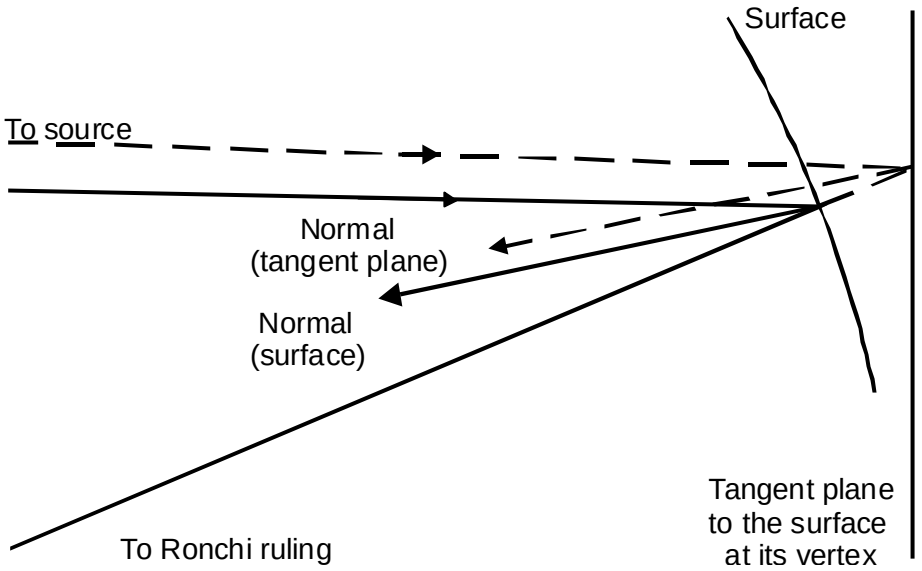

Once the local normals to the surface were calculated, the last step consisted in performing the final topographic reconstruction through the surface integration procedures described in Section 4.2.5. The final data obtained provides us with a new method for measuring the radius of curvature of the sample, which has up to now only been measured through two-dimensional curve-fitting. A three-dimensional sphere following

$$z = \frac{\frac{\sqrt{(x-x_0)^2+(y-y_0)^2}}{R}}{1+\sqrt{1-(\frac{(x-x_0)^2+(y-y_0)^2}{R^2})}} \qquad (6.2.1)$$

may be fitted to the reconstructed surface through three-dimensional curve-fitting software, giving the values for the radius of curvature and the positioning of the center of the surface listed in Table 6.2.5 for the microstepped and non-microstepped measurement. Notice how the angular misalignment term of the two-dimensional fitting procedures has turned into a position misalignment measurement in three-dimensional curve-fitting procedures, in the form of the (x_0,y_0) coordinates of the vertex of the surface. The position misalignment along the X axis is much greater than the one along the Y axis, as was already known from the results of two-dimensional fitting and from

the $y_R(x_R)$ and the $y_S(x_S)$ plots. The correlation coefficients are still highly satisfactory, and the results agree very well with the ones obtained through two-dimensional curve-fitting procedures.

Table 6.2.5: Result for the fitting of the reconstructed surface to Eq. 6.2.1.

Sample P175 A	R(mm)	x_0(mm)	y_0(mm)	r^2
Non-microstepped	149.78	0.66	0.03	0.999998
Microstepped	149.78	0.66	0.03	0.999998

One highly relevant feature is the very small differences obtained in the measurement of the radius of curvature when comparing microstepped and non-microstepped procedures, a result which was previously observed in two-dimensional fitting procedures. It may be affirmed that if our goal was just to obtain such radius of curvature measurements, the use of microstepping techniques would not yield any important improvement to the measured value. Thus, in the event of the technique being applied to the measurement of radius of curvature of surfaces, microstepping techniques would not improve the measurement and should not be applied because of the great increase in measurement and computation time they entail.

Fig. 6.2.12 presents a three-dimensional topographic reconstruction of the measured sphere, together with a plot of the residuals of the measured data relative to the best fit sphere. The latter is a plot of the measured deformations of the tested surface. Microstepped and non-microstepped measurements are also presented. It may be seen how both measurements display similar results, although an intensive sampling on the surface was performed in the microstepped experiment, which is revealed by the amount of data points plotted on the surface. In the case of microstepping, the shape of the resulting surface could be extracted without any surface interpolation from the large amount of sampling points available. Residual plots display a very interesting toroidal shape, with residuals of the sampling points under $\pm 5\mu m$ from the best fit sphere, which will be recalled in Section 6.2.3 and 6.3. The sampled surface area is $204mm^2$; and the measured height range amounts to 0.36mm. A complete error analysis with standard deviations and confidence intervals of the fitted values will be performed in Section 6.2.2.

Fig. 6.2.12: Three-dimensional surface plots of : (a) Best fit sphere, non-microstepped measurement; (b) Residuals from the best fit sphere, non-microstepped measurement; (c) Best fit sphere, microstepped measurement; (d) Residuals from the best fit sphere, microstepped measurement.

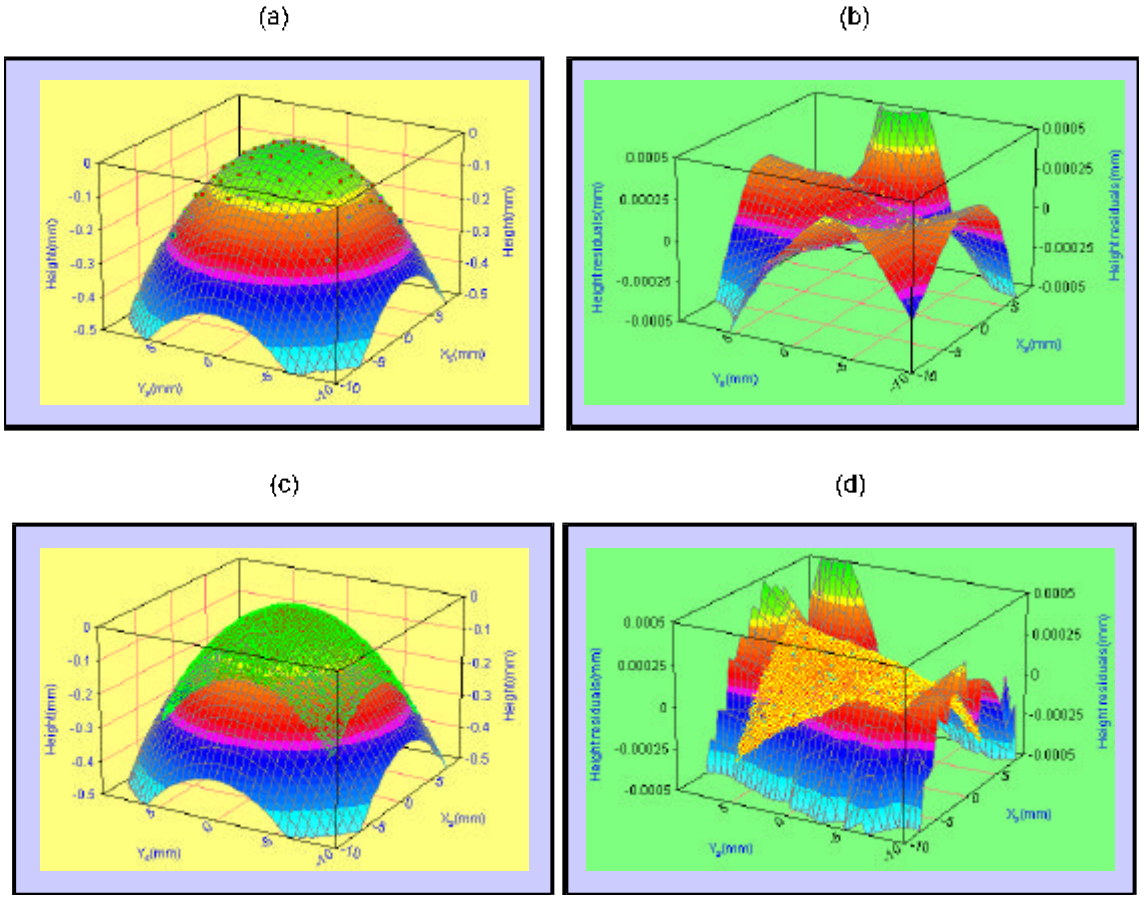

Fig. 6.2.13 contains a pseudocolor contour plot of the reconstructed topography of the surface, with contour levels increasing in 18μm steps in the non-microstepped experiment and 22μm steps in the microstepped one. The residuals from the best fit sphere are also plotted, with contour levels increasing in 11nm steps in the non-microstepped and 36nm steps in the microstepped measurement. It should be noted that this nanometric accuracy is merely a numerical result of our interpolation procedures. The blue level presented in the residual plot equals the zero deviation from the best fit sphere. Each sampled point is an active pixel in a 256x256 pixel matrix in the microstepped experiment, with its color determined by its height value. In the non-microstepped experiment, each pixel has been enlarged to a 5x5 pixel block in order to make them more visible.

Fig. 6.2.13: Pseudocolor plots of (a) Measured spherical surface, non-microstepped measurement; contour levels are plotted in 18μm steps; (b) Residuals from the best fit sphere, non-microstepped measurement; each contour step equals 11nm; (c) Measured spherical surface, microstepped measurement; each contour step equals 22μm (d) Residuals from the best fit sphere, microstepped measurement; each contour step equals 36nm. Each plotted point is a measured data point. Data points in the non-microstepped experiment have been enlarged.

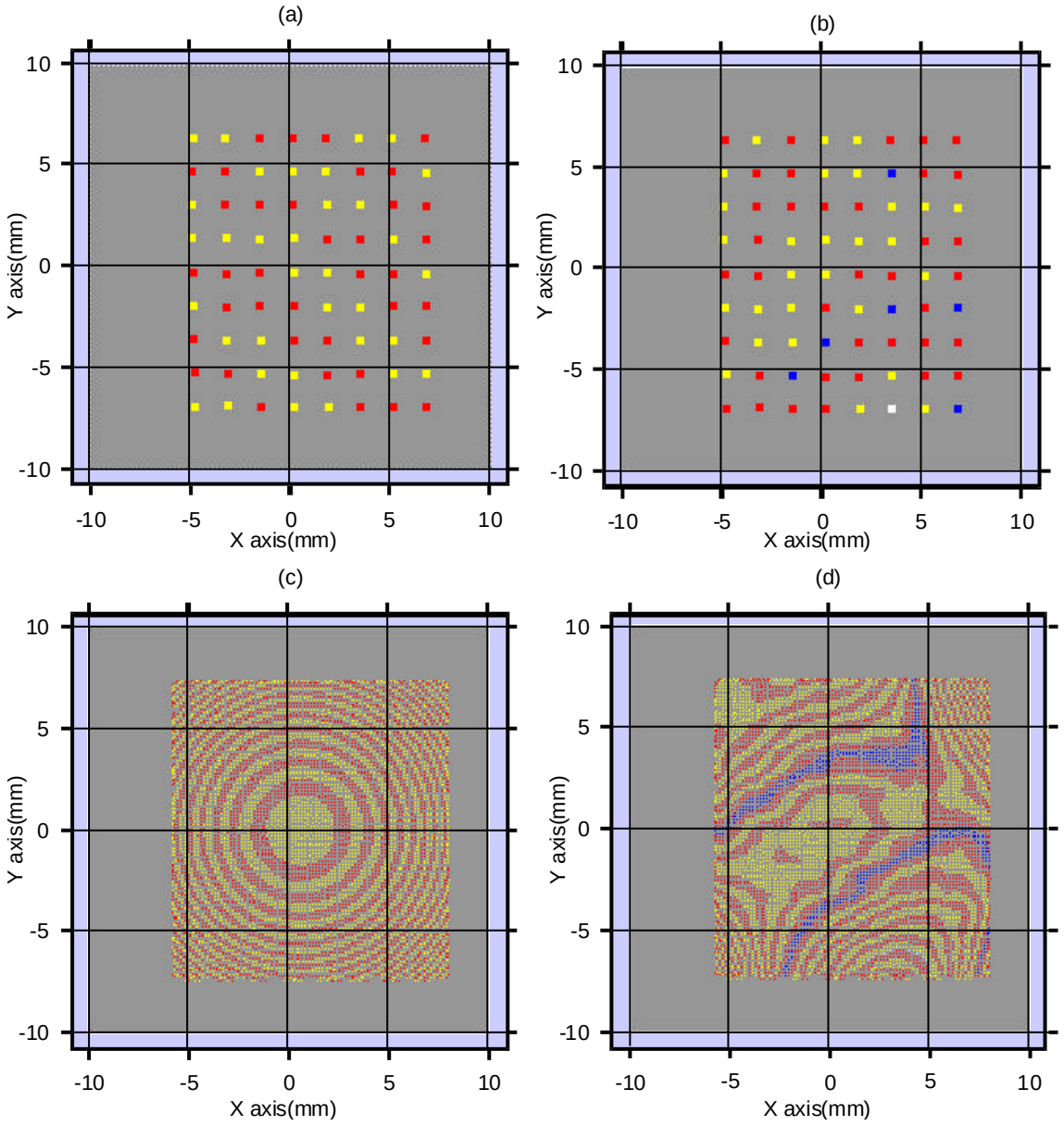

Despite the fact that Fig.6.2.13 might be less visually appealing than Fig.6.2.12, we understand this sort of pseudocolor plots provide more detailed information than the three-dimensional plots previously presented, because the perspective effects associated with plotting a three-dimensional plot on two-dimensional paper are avoided. Another obvious conclusion which can drawn from Fig. 6.2.13 is that, although

microstepped and non-microstepped measurements may be nearly equivalent when measuring curvature values, the quality of the surface topographies and residuals obtained is very much improved when using microstepping techniques, as more information from the surface is available in the topographic reconstruction of the surface, and the data residuals from the best fit sphere allow the measurement of submicrometric surface features

Consequently, in order to reduce the amount of information and plots provided for each of the remaining samples, surface topographies in Section 6.3 will only be provided as pseudocolor plots, and only microstepped measurements and residuals from the best fit surface will be presented. None of the intermediate graphs presented in this typical measurement example will be provided, as other surface topographies will only differ from the one depicted in the present section in some numerical values, and they would not provide us with any additional information. For this reason each measurement process like the one presented here will be summarized in Section 6.3 by means of a Table containing some experimental parameters together with the two-dimensional and three-dimensional curve-fitting numerical results, and by the pseudocolor plots of the reconstructed topography and the residuals from the best fit sphere obtained in the microstepped experiment.

6.2.2.- Error analysis

In Section 4.3 the accuracy of the measurement technique was analyzed from two points of view. In Section 4.3.1 the accuracy of each individual measurement was estimated, yielding a typical measured value of $C= 8.61\ 10^{-3} \pm 1.8\ 10^{-4}$ mm^{-1}. The curvature values obtained in our measurement of sample P175A (around $6.67\ 10^{-3}$ mm^{-1}, depending on the axis considered and on whether microstepping was applied, see Table 6.2.3) in fact stay close to this assumption.

However, in Section 4.3.2, the overall accuracy in the measurement of curvature through curve fitting procedures was theoretically presented (Eq.4.3.7), though not calculated, as it was shown to be numerically dependent on the experimental data available. This Section provides complete numerical results for the experimental data obtained in the measurement of sample P175A in position P1, as part of the measuring process being carried out in Section 6.2.

Numerical results for the error in the measurement of curvature values using two-dimensional curve-fitting are presented in Table 6.2.6, displaying values for the

standard deviation of the fitted curvature values, its relative importance for the curvature value, the confidence interval where the real curvature value of the surface may be found with a probability of 0.95 (eq.4.3.7), and the radius of curvature change within the interval of variation of C±σ.

Table 6.2.6: Error analysis in two-dimensional curve-fitted curvature values for the X and Y directions of the non-microstepped and microstepped experiments. σ stands for the standard deviation of the data, %σ for its relative error, C_{MIN}^{95} and C_{MAX}^{95} for the limits of the confidence interval where the real curvature value is found within a probability of 0.95, R for the radius of curvature and ΔR for its variation in the interval of curvatures C±σ.

Sample P175 A	**C (mm^{-1})**	**s (mm^{-1})**	**%s**	C_{MIN}^{95} **(mm^{-1})**	C_{MAX}^{95} **(mm^{-1})**	**R (mm)**	**ΔR (mm)**
$N_X(x_S)$; non-μst.	$6.6750\ 10^{-3}$	$1.1\ 10^{-6}$	0.016	$6.6728\ 10^{-3}$	$6.6772\ 10^{-3}$	149.81	0.049
$N_Y(y_S)$;non-μst.	$6.6678\ 10^{-3}$	$7.0\ 10^{-7}$	0.010	$6.6665\ 10^{-3}$	$6.6692\ 10^{-3}$	149.97	0.031
$N_X(x_S)$; μstepped	$6.6759\ 10^{-3}$	$1.2\ 10^{-7}$	0.002	$6.6757\ 10^{-3}$	$6.6761\ 10^{-3}$	149.79	0.005
$N_Y(y_S)$; μstepped	$6.6684\ 10^{-3}$	$7.2\ 10^{-8}$	0.001	$6.6682\ 10^{-3}$	$6.6685\ 10^{-3}$	149.96	0.003

Standard deviation values may be seen to be very small, both in their relative and absolute values, which is a consequence of the very good correlation coefficients obtained in the linear regression(see Table 6.2.3). The confidence intervals are also very narrow, with the radius of curvature variations in the 0.95 probability interval being of only some micrometers. An advantage of microstepping procedures in measuring curvatures can be observed for the first time, as smaller standard deviations and confidence intervals are obtained. This is a direct effect of the higher number of data points, predicted from Eq.4.3.7, where the uncertainty in the determination of the coefficients in the linear regression was seen to depend on $1/\sqrt{N}$, N being the number of sampled points. By using microstepping procedures N has risen from 73 to 7583, providing the ten-fold reduction in standard deviation and confidence intervals obtained.

Errors in the measurement of the angular misalignment of the surface can also be measured this way, and are presented in Table 6.2.7. Although their relative values are more important than for the curvatures measured, they are also much lower values. The same kind of effect of the number of data points on standard deviation may be observed when comparing microstepped and non-microstepped measurements.

Table 6.2.7: Errors in two-dimensional curve-fitted angular misalignment values for the X and Y directions of the non-microstepped and microstepped experiments. σ stands for the standard deviation of the data, $\%\sigma$ for its value relative to the measured value, K_{MIN}^{95} and K_{MAX}^{95} for the limits of the interval where the real angular misalignment value is found within a 0.95 probability.

Sample P175 A	**K(rad)**	**σ (rad)**	**$\%\sigma$**	**K_{MIN}^{95} (rad)**	**K_{MIN}^{95} (rad)**
$N_X(x_S)$; non-µstep.	$-4.4088\ 10^{-3}$	$4.3\ 10^{-6}$	0.10	$-4.4174\ 10^{-3}$	$-4.4001\ 10^{-3}$
$N_Y(y_S)$;non-µstep.	$-2.1046\ 10^{-4}$	$3.0\ 10^{-6}$	1.43	$-2.1645\ 10^{-4}$	$-2.0447\ 10^{-4}$
$N_X(x_S)$; µstepped	$-4.4105\ 10^{-3}$	$5.2\ 10^{-7}$	0.01	$-4.4115\ 10^{-3}$	$-4.4095\ 10^{-3}$
$N_Y(y_S)$; µstepped	$2.0516\ 10^{-4}$	$3.1\ 10^{-7}$	0.15	$-2.0576\ 10^{-4}$	$-2.0456\ 10^{-4}$

A complementary error analysis may be performed through three-dimensional curve fitting procedures. In this case, however, the parameters to obtain through curve-fitting are the radius of curvature and the position of the vertex of the spherical surface considered. The standard deviations and confidence intervals for the measured parameters are now related to a full surface fitting, instead of being merely a linear regression fitting which involves independent curvatures along the X and Y axes. Error analysis for the three-dimensional radius of curvature fitting and the measured vertex position in non-microstepped and microstepped measurements are presented in Table 6.2.8.

The conclusions that may be drawn from this table are similar to the ones obtained in the error analysis from two-dimensional fitting. Microstepped measurements yield a better standard deviation because of the higher number of data points involved, although the relative error of the non-microstepped measurement is only 0.018% (1 part in 56) of the measured value of the radius of curvature. Small errors may also be found in the measurement of the position of the surface vertex, with the relative error in the measurement of y_o being slightly larger on account of its small measured value.

From the results presented we may estimate the total uncertainty of the measurement technique, which has been shown to be mainly due to the uncertainties of the experimental setup in the measurement of a single slope value. The uncertainty in the fitting procedures is much smaller, meaning the measured data presents very little dispersion from the central values. That is, the global uncertainty of the measurements is the estimated value presented in Section 4.3.1, which has a relative value of $\pm 2\%$ of

the measured value ($C=8.61\ 10^{-3} \pm 1.8\ 10^{-4}\ mm^{-1}$). However, such a value should be considered to be an overestimate, as in following Sections the experimental data obtained will be seen to be closer than a 2% to the reference values.

Table 6.2.8: Error analysis for the radius of curvature and the vertex of the sample surface position from three-dimensional fitting. σ stands for standard deviation, $\%\sigma$ for its relative value and ξ for the variable considered in the corresponding row.

Sample P175 A		**Fit**	σ	**%** σ	ξ_{95}^{MIN}	ξ_{95}^{MAX}
R (mm)	Non-μstep.	149.78	$27.\ 10^{-3}$	0.018	149.72	149.83
	μstepped	149.78	$2.4\ 10^{-3}$	0.002	149.78	149.79
x_0 (mm)	Non-μstep.	0.6608	$4.6\ 10^{-4}$	0.070	0.6600	0.6618
	μstepped	0.6609	$4.3\ 10^{-5}$	0.007	0.6608	0.6609
y_0 (mm)	Non-μstep.	0.0319	$4.0\ 10^{-5}$	0.125	0.0311	0.0327
	μstepped	0.0307	$3.3\ 10^{-6}$	0.011	0.0306	0.0307

In order to go on reducing the vast amount of data available for each experimental measurement, in this Section it has been seen how the information provided for the error analysis in two-dimensional and three-dimensional fitting procedures gives similar information about the dispersion of the measured data. On account of this, in Section 6.3 two and three-dimensional fitted values for all spherical surfaces will be presented, but error analysis data will only be presented from three-dimensional fitting procedures. This kind of procedures has been preferred for simultaneously taking into account the data values available along both axes, and not merely a z(x) or z(y) projection of the data along one or the other of the reference axes.

6.2.3.- Validity of the measured value

Finally, a reference measurement will be presented in order to compare its result with the one obtained using the Ronchi test technique. A Möller-Wedel Measuring Combination V used in its high precision radioscope configuration was used in order to measure the radius of curvature of the P175A surface. The accuracy of the instrument is 0.1mm in the measurement of radius of curvature.